Metal-Organic frameworks encapsulated Ag Nanoparticle-Nanoclusters with enhanced luminescence for simultaneous detection and removal of Chromium(VI)

Hao Yuan, Huangmei Zhou, Yu Zhao, Hao Tan, Rodolphe Antoine, Sanjun Zhang

Metal-Organic Frameworks Encapsulated Ag Nanoparticle-Nanoclusters with Enhanced Luminescence for Simultaneous Detection and Removal of Chromium(VI)

Hao Yuan[†], Huangmei Zhou[†], Yu Zhao[†], Hao Tan[†], Rodolphe Antoine*[, §], and Sanjun Zhang*[, †, ‖]

[†] State Key Laboratory of Precision Spectroscopy, East China Normal University, No.500, Dongchuan Rd., Shanghai 200241, China

[§] Institut Lumière Matière UMR 5306, Université Claude Bernard Lyon 1, CNRS, Univ Lyon, F69100 Villeurbanne, France

[‖] Collaborative Innovation Center of Extreme Optics, Shanxi University, Taiyuan, Shanxi 030006, China

***Corresponding Author**

E-mail addresses: R.A.: rodolphe.antoine@univ-lyon1.fr; S.Z.: sjzhang@phy.ecnu.edu.cn

Abstract:

Metal nanoclusters (NCs) have emerged as a class of promising luminescent materials for sensing, but the low luminescence efficiency hindered their applications. In this work, highly luminescent composites were synthesized by encapsulating D-penicillamine (DPA) capped silver nanoparticle-nanoclusters (AgNP-NCs) into zeolitic imidazolate frameworks (ZIF-8) (denoted as AgNP-NCs@ZIF-8) and were applied for simultaneous detection and removal of chromium(Ⅵ). The photoluminescence intensity of the AgNP-NCs was enhanced by (66 ± 5) folds due to the confinement of ZIF-8 shell, and the lifetime was prolonged from (50.9 ± 1.8) ns to (15.9 ± 0.4) μs. More importantly, thanks to the strong luminescent property of AgNP-NCs and porous structure of the ZIF-8 shell, the AgNP-NCs@ZIF-8 composites not only allowed for the detection of Cr(Ⅵ) as luminescent probe but also exhibited good adsorption capacity of Cr(Ⅵ). The luminescence intensity decreased linearly with Cr(Ⅵ) concentration in the range of 40 to 400 μM, and the limit of detection was determined to be (23.5 ± 0.8) μM. They also exhibited high selectivity toward total chromium in various interfering metal ions and good performance in real water samples. These results indicated that AgNP-NCs@ZIF-8 could serve as an attractive candidate for simultaneous detection and removal of Cr(Ⅵ) in environmental monitoring and protection.

Keywords:

silver nanoclusters, metal-organic frameworks, luminescence enhancement, photoluminescence detection, removal, chromium(VI)

1 Introduction

Luminescent metal nanoclusters (NCs) display amazing photoluminescence (PL) features, including tunable luminescence, large Stokes shift, and good photo-stability. Significant progress has been achieved in the elaboration of NCs-based sensors for specific analytes in recent years [1, 2]. However, the luminescence of most metal NCs is usually weak, which seriously hinders their applications. Therefore, efforts have been devoted to enhancing the luminescence of metal NCs [3]. Based on aggregate-induced emission enhancement (AIEE), popular strategies to enhance the luminescence of NCs were developed [4], such as ligand-shell rigidifying [5], solvent-induced aggregation [6], ion-induced aggregation [7], and spatial confinement [8], etc. Recently, metal nanoparticles supporting surface plasmon resonance (SPR) has also been applied to enhance the emission of NCs, known as plasmon-enhanced fluorescence (PEF) effect [9, 10]. It is hypothesized that if PEF and AIEE could be incorporated into the same metal NC system, the luminescence efficiency may be further improved due to their synergistic effect.

Metal-organic frameworks (MOFs), as nanomaterials with various advantages and functions, possess tunable pores to accommodate various types of guest species, such as dyes [11], enzymes [12], metal nanoparticles [13], and metal NCs [14, 15], etc. The encapsulation of metal NCs into MOFs (denoted as NCs@MOF) has been reported to intensify the luminescence because NCs were confined in the rigid structure of MOFs [16]. Successful examples, such as AuNCs@ZIF-8 [17-19], CuNCs@ZIF-8 [20], and CuNCs@ZIF-90 [21], exhibited excellent photoluminescence and detection performance. It would be possible to obtain composites with synergistic effect of PEF and AIEE by support of metal nanoparticles and encapsulation of metal-organic frameworks. Moreover, the porous structure of MOF shells endows NCs@MOF with additional adsorption capability, which benefits the removal of toxic pollutants from the environment [22, 23]. Hence, owing to the

improved PL performance of NCs and porous structure of MOF shell, NCs@MOF can be considered as a type of promising candidate for simultaneous photoluminescence detection and adsorptive removal of environmental pollutants.

Chromium(Ⅵ), the most harmful metal ion pollutant [24], can easily enter cells, damage organisms, and threaten human health [25]. Therefore, it is urgently needed to develop advanced strategies for Cr(VI) detection and removal from the environment, especially for simultaneous detection and removal of Cr(Ⅵ) [26]. Recently, these multifunctional platforms have been constructed. For example, layered double hydroxide composites, coumarin and resorufin dye-containing MOF-801 composites have been reported to be successfully designed for luminescence detection and simultaneous removal of Cr(Ⅵ) [26-28].

In this study, we encapsulated D-penicillamine capped silver nanoparticle-nanoclusters (AgNP-NCs) into zeolitic imidazolate frameworks (ZIF-8) to obtain novel AgNP-NCs@ZIF-8 composite and applied them for simultaneous detection and adsorptive removal of Cr(Ⅵ) as illustrated in Scheme 1. The AgNP-NCs@ZIF-8 exhibited synergistic PEF and AIEE effects, which was considered as a creative luminescence enhancement method for nanoclusters. The luminescence intensity of the AgNP-NCs@ZIF-8 was significantly improved by (66 ± 5) folds compared to that of AgNP-NCs. When the AgNP-NCs@ZIF-8 composites were applied for simultaneous luminescence detection and adsorptive removal of Cr(Ⅵ) in water, they showed not only excellent performance in detection of Cr(Ⅵ) but also a good adsorption capacity of Cr(Ⅵ). To the best of our knowledge, this is the first report on NCs@MOF for simultaneous detection and effective removal of environmental pollutants from water so far.

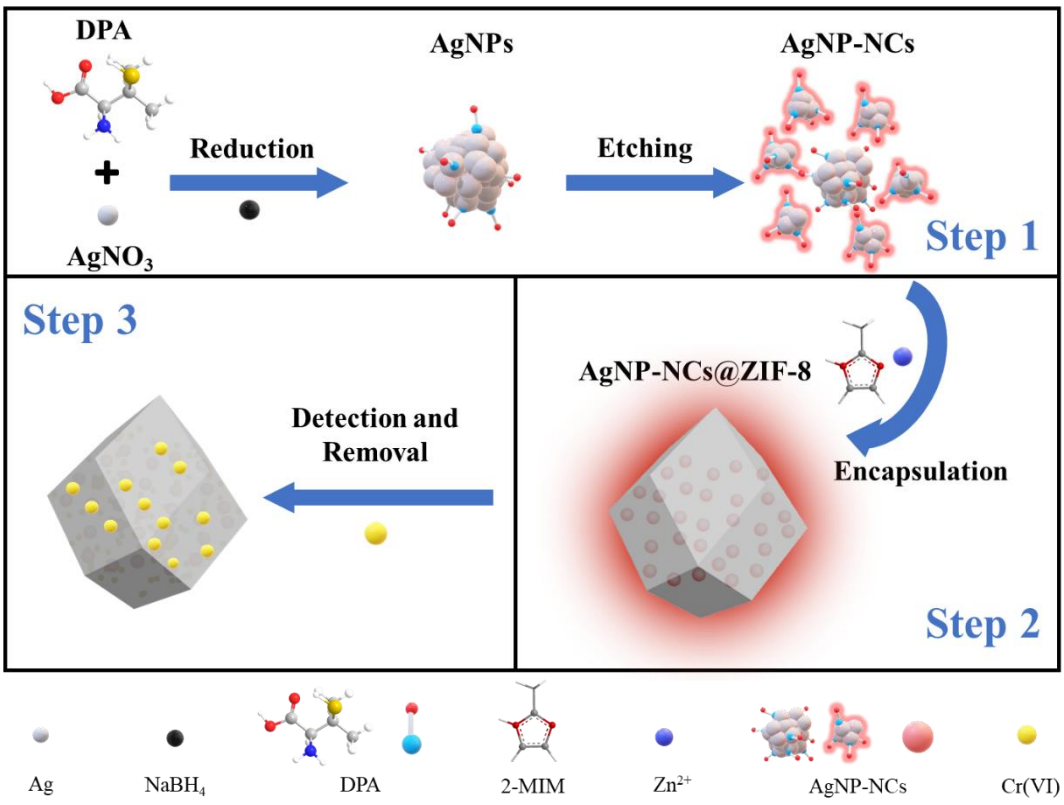

Scheme 1. Schematic illustration of the synthesis of AgNP-NCs (Step 1), AgNP-NCs@ZIF-8 (Step 2) composites, and their applications in Cr(Ⅵ) detection and removal (Step 3).

2 Experimental section

2.1 Materials and Reagents

Silver nitrate ($AgNO_3$), zinc nitrate hexahydrate ($Zn(NO)_3•6H_2O$), dimethyl imidazole (2-MIM), potassium dichromate ($K_2Cr_2O_7$), metal nitrate salts, hydrogen peroxide (H_2O_2), sodium hydroxide (NaOH), and ethanol were purchased from Sinopharm Chemical Reagent Co., Ltd. (Shanghai, China). D-penicillamine (DPA) was purchased from Aladdin (Shanghai, China). Sodium borohydride ($NaBH_4$) was obtained from Sigma-Aldrich (Shanghai, China). Ultrapure water (resistivity of 18.2 MΩ•cm^2) was used throughout all experiments. All the reagents were used as received

without further purification.

2.2 Instrumentation and Characterization

Transmission electron microscopic (TEM) and high-resolution transmission electron microscopic (HRTEM) images were collected on a JEOL JEM-2100F transmission electron microscope (JEOL, Japan) operating at 200 kV. Fourier transform infrared (FTIR) spectroscopy was performed with a NICOLET iS10 Infrared Spectrometer (Thermo Fisher Scientific, USA). Dynamic light scattering (DLS) was measured by Zetasizer Nano ZS ZEN 3600 (Malvern Instruments Ltd., UK). The circular dichroism (CD) spectra were collected on a J-1500 CD spectrometer (JASCO, Japan). UV-Vis absorption spectroscopy was performed with a two-beam TU-1901 UV-Vis spectrometer (PERSEE, China). All steady-state luminescence measurements were carried out on a FluoroMax-Plus photoluminescence spectrometer (Horiba, Japan). Luminescence lifetime of AgNP-NCs was measured with a homebuilt time-correlated single photon counting (TCSPC) system with a time resolution of about 200 ps [29]. The luminescence lifetime of AgNP-NCs@ZIF-8 was measured on an FLS 980 spectrofluorometer (Edinburgh Instruments, UK) equipped with a μF2 lamp. Femtosecond transient absorption (TA) spectra were measured on a spectrometer (Helios Fire, Ultrafast System, USA) with a 350 nm pump beam generated by a Ti:sapphire laser system (Astrella, 800 nm, 100 fs, 7 mJ/pulse, and 1 kHz, Coherent Inc., USA). A fraction of the laser fundamental beam was focused into a sapphire to generate a white light continuum over 400 nm to 740 nm as the probe beam. All experiments were carried out at room temperature.

2.3 Synthesis of AgNP-NCs

The AgNP-NCs were synthesized by a reduction-etching process. Aqueous

solution of DPA (0.5 M, 0.4 mL) and freshly prepared aqueous solution of $AgNO_3$ (0.1 M, 0.5 mL) were added to 4.8 mL ultrapure water. Under vigorous stirring, freshly prepared $NaBH_4$ ice-cold solution (0.625 mM, 0.16 mL) was added to the above mixture. The colorless transparent solution turned brown-black immediately. With continuous stirring, the solution gradually turned from brown-black to bright yellow. After etching for 7 h, a transparent yellow aqueous solution of AgNP-NCs was formed. The stirring was stopped and the prepared AgNP-NCs were used for further MOF encapsulation. The reaction time needed to be precisely controlled for reproducibility.

2.4 Synthesis of AgNP-NCs@ZIF-8

The 1 mL as-prepared aqueous solution of AgNP-NCs was mixed with 6 mL 25 mM $Zn(NO)_3$•$6H_2O$ aqueous solution. Then, 6 mL 75 mM 2-MIM aqueous solution was added into the mixture and stirred at room temperature for 20 min. The reacted mixture turned milky, and red emission could be observed under UV radiation. The product was centrifuged, washed three times with ethanol, and then dried overnight in vacuum to obtain the light-yellow powder.

2.5 Luminescence detection and removal of chromium(Ⅵ)

For Cr(Ⅵ) detection, 1 mL of 1 mg/mL fresh-prepared AgNP-NCs@ZIF-8 colloidal aqueous solution was mixed with 300 μL $K_2Cr_2O_7$ solution of different concentrations. The total solution volume was diluted to 3 mL with ultrapure water. The pH of Cr(Ⅵ) solution and ultrapure water was adjusted to 8.5 by NaOH solution, the same as that of AgNP-NCs@ZIF-8 solution. According to the optimum excitation and emission wavelength, the emission spectra and PL intensity at 730 nm were measured at an excitation wavelength of 420 nm after incubating at room temperature for 10 h. Of note, the luminescence of solid powder could last for more than half a

year while the colloidal solution in water was not stable enough. Therefore, it was necessary to prepare the AgNP-NCs@ZIF-8 aqueous solution on the same day and precisely control the concentration (1 mg/mL) for good performance in application.

Similar to the procedure of luminescence detection, the adsorption experiments were conducted by mixing AgNP-NCs@ZIF-8 solution with Cr(Ⅵ) solution of 5, 25, 50, 200, 667 μM. The pH of Cr(Ⅵ) solution was also adjusted to 8.5 in advance. After 10 h, the AgNP-NCs@ZIF-8 sorbent was centrifuged from the solution. The Cr(Ⅵ) concentration was determined by the typical absorbance of $Cr_2O_7^{2-}$ at 370 nm and the adsorption capacity of AgNP-NCs@ZIF-8 was evaluated by the following equation:

$$Q_e = \frac{C_0 - C_1}{m} \times V_{solution}$$

where Q_e represents the adsorption capacity of AgNP-NCs@ZIF-8; C_0 and C_1 represent the Cr(Ⅵ) concentration before and after adsorption, respectively; m represents the weight of sorbent and $V_{solution}$ represents the volume of solution.

For selectivity experiment, aqueous solutions of metal nitrate salts (Na^+, Ca^{2+}, Zn^{2+}, Cr^{3+}, Co^{2+}, Cd^{2+}, Ni^{2+}, Pb^{2+}, Cu^{2+}, K^+, Mg^{2+}, Mn^{2+}, Fe^{3+}, Ag^+, and Hg^{2+}) were added instead of Cr(Ⅵ) to a final concentration of 25 μM. For a good selectivity toward chromium, the solutions of Cr(Ⅲ), Cr(Ⅵ), and Cu^{2+} were pretreated with H_2O_2 in NaOH solution (pH=8.5) at 60 ℃ for 30 min, where the molar ratio of H_2O_2 to metal ions was 5:1. Then the mixtures were centrifuged for 10 min at 12000 rpm. The supernatant was collected for the selectivity experiment. A control experiment was also performed at the same time.

In a typical interference experiment, Cr(Ⅵ) solution was added into four random groups of aqueous solutions containing different mixed metal ions, m1: Na^+/Ca^{2+}/Fe^{3+}, m2: K^+/Co^{2+}/Mn^{2+}, m3: Mg^{2+}/Ag^{2+}/Pb^{2+}, m4: Zn^{2+}/Ni^{2+}/Cd^{2+}. The concentration of Cr(Ⅵ) and all the interference metal ions was 100 μM. The mixtures were prepared for luminescence measurements. In the detection and removal experiments, three samples were prepared and the experiments were repeated under the same condition for the repeatability.

2.6 Luminescence detection of chromium(Ⅵ) in real samples

To assess the practical applicability for Cr(Ⅵ) detection, the drinking water and the tap water were collected. The drinking water was purchased from Watsons water (Guangzhou, China) and tap water was obtained from the Optics Building on the Minhang campus of East China Normal University. The pH of all water samples was adjusted to 8.5 with NaOH, then Cr(Ⅵ) in water samples was detected by spiking known amount of Cr(Ⅵ) at three different concentrations (50, 100, 200 μM) with AgNP-NCs@ZIF-8 as fluorescent sensor. And the experiment was repeated three times for each spike level.

3 Results and Discussion

3.1 Preparation and Characterization of AgNP-NCs

We first synthesized DPA-capped AgNP-NCs by a reduction-etching process as illustrated in Scheme 1. The absorption and fluorescence spectra were characterized during the reaction to reveal their unique nanoparticle-nanocluster compositions (Fig. 1a and Fig. S1). After the addition of reductant to the mixture of Ag^{+} and ligand, a strong surface plasmon resonance (SPR) absorption peak close to 410 nm was observed in the absorption spectrum (Fig. S1a), and the large AgNPs were non-luminescent. As the large Ag nanoparticles were etched by the thiolated ligands (DPA), a number of small luminescent AgNCs formed. The photoluminescence intensity increased with etching time and reached maxima after 7 hours (Fig. S1b and S1c). When the etching continued to proceed, the photoluminescence intensity started to decrease and the plasmonic absorbance peak decreased as well. The system became non-luminescent after 24 hours. Thus, the reaction time for maximum photoluminescence intensity was optimized to be 7 hours, and the optimal molar ratio

of DPA to Ag was obtained to be 4:1 by observing the photoluminescence intensities (Fig. S2).

The AgNP-NCs prepared under the optimal synthesis conditions (DPA/Ag=4:1, etching time 7 h) were further characterized in detail. The formation of DPA-capped AgNP-NCs was confirmed by FTIR. The peak at 2605 cm^{-1}, corresponding to the S-H stretching vibration of DPA, disappeared in FTIR spectrum of AgNP-NCs (Fig. S3). This change in FTIR spectra indicated that the S-H bonds were broken and the DPA ligands were anchored on Ag atoms through S-Ag bonds. The absorption spectrum showed an absorption peak at 410 nm (Fig. 1b), which was consistent with surface plasmon resonance (SPR) absorption peak of AgNPs [30], indicating the plasmonic feature of these AgNP-NCs. Of note, the molecular-like liganded nanoclusters present multiple bands at wavelengths longer than 410 nm [31, 32]. The AgNP-NCs showed an emission peak at 665 nm (Fig. 1c). The sharp excitation peak at 410 nm (Fig. 1c) overlapped with the SPR peak of AgNPs, so we speculated the luminescence excited at 410 nm originated from plasmon-enhanced fluorescence (PEF) of luminescent nanoclusters. Metal nanoparticles have been demonstrated to enhance the luminescence of various fluorophores due to PEF [33]. TEM image showed that the AgNP-NCs exhibited dot-like morphologies and broad size distribution from 1.6 nm to 4.4 nm (Fig. 1d). The HRTEM showed that the lattice fringes had a spacing of 0.23 nm (Fig. S4), corresponding to the (111) plane of metallic Ag. Size histograms obtained from DLS measurements showed the hydrodynamic diameter was 2.2 nm (Fig. 1e), consistent with the results of TEM. AgNPs with diameters larger than 2-3 nm can support SPR. To further confirm the plasmonic effect of the AgNP-NCs, we probed the electron dynamics of AgNP-NCs by pump intensity-dependent femtosecond transient absorption spectroscopy. As the pump intensity increased from 50 μW to 200 μW, the AgNP-NCs exhibited pump power-dependent dynamics (Fig. 1f). This result corroborated the plasmonic feature of AgNP-NCs, due to the fact that the initial electron temperature of metallic-state particles is highly dependent on the

pump laser intensity, and the electron dynamics is thus pump power-dependent [34-36]. The plasmonic feature existing in large AgNPs and the luminescent feature existing in small AgNCs can be reconciled by a simple core-shell structure with large AgNPs as the core and small AgNCs as the shell as illustrated in Scheme 1. Note that besides the core-shell structure, the superstructure of AgNCs may also be a reasonable explanation [37], but it is out of the scope of this investigation to discuss the plasmonic effect originating from AgNPs or AgNC superstructures. Since this system exhibited a pronounced hybrid feature of large plasmonic AgNPs and small luminescent AgNCs, we denoted this system with AgNP-NCs. It can be observed that the PEF not only enhanced the emission intensity but also shifted the optimal excitation wavelength from UV to visible region, which benefits the applications of the AgNP-NCs.

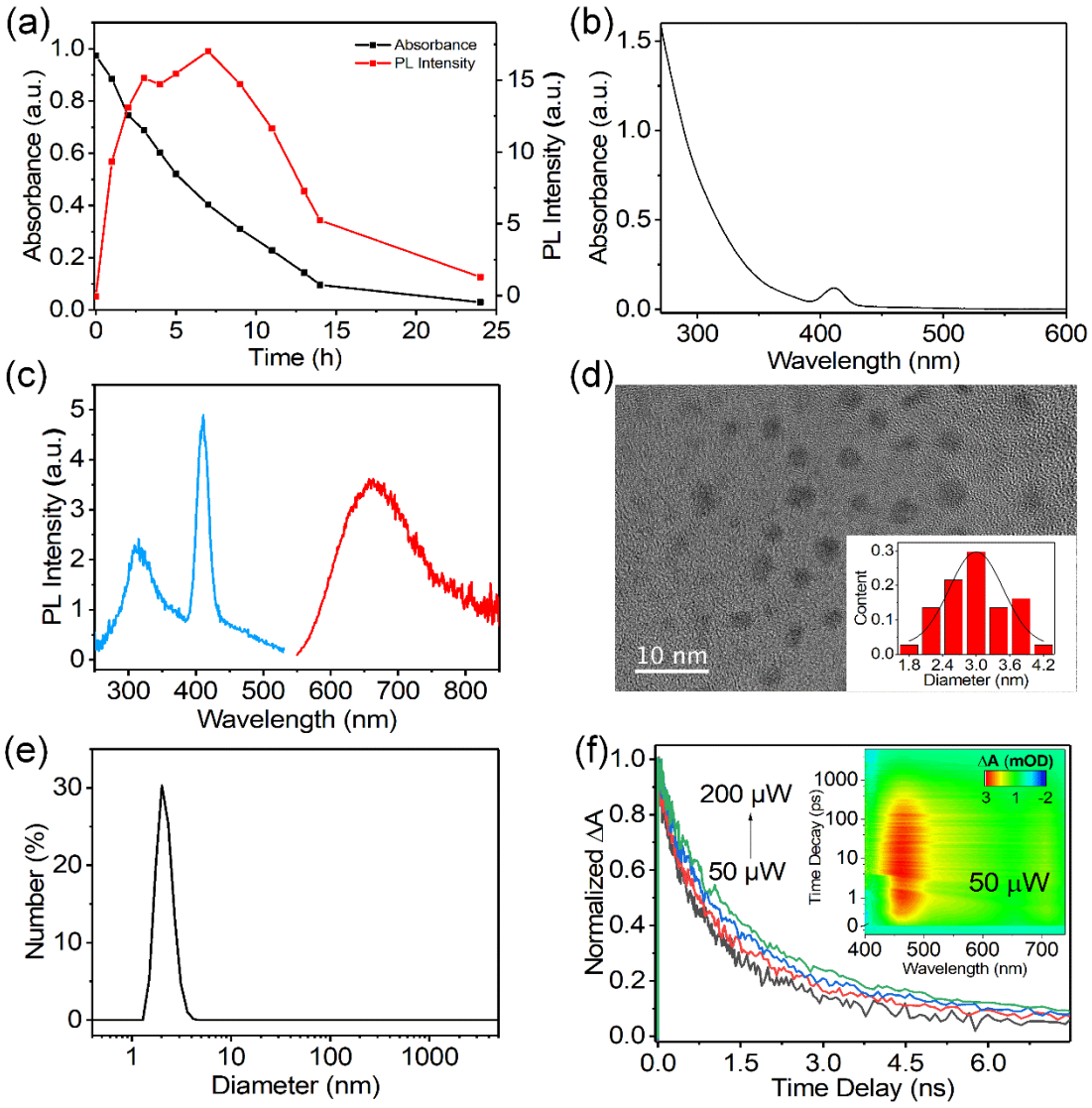

Fig. 1. (a) Variation of PL intensity (red line, λ_{ex} = 410 nm.) and absorption peak intensity (black line, observed at 410 nm) of AgNP-NCs versus reaction time. (b) UV-Vis absorption spectrum of the AgNP-NCs. (c) Excitation and emission spectra of the AgNP-NCs (λ_{ex} = 410 nm, λ_{em} = 665 nm). (d) TEM image and size distribution (inset) of the AgNP-NCs. (e) Hydrodynamic size distribution of the AgNP-NCs obtained by DLS technique. (f) Normalized decay kinetics as a function of pump intensity influence for AgNP-NCs excited at 350 nm and monitored at 456 nm. Inset: Transient absorption data map of the AgNP-NCs with 50 μW pump influence.

3.2 Preparation and characterization of AgNP-NCs@ZIF-8

To harness the AIEE effect to enhance the luminescence of NCs by encapsulating them into MOF, it is required that the NCs should have AIEE effect. The AgNP-NCs were first measured to have AIEE effect prior to MOF encapsulation. As demonstrated in Fig. S5a, the photoluminescence intensity of the water-soluble AgNP-NCs was dependent on the proportion of ethanol ($f_e=V_{ethanol}/V_{ethanol+water}$) in a mixed ethanol-water solvent. Similar to the phenomena observed in other water-soluble AIEE nanoclusters [38-40], the photoluminescence intensity of the AgNP-NCs gradually increased with increasing f_e. Solvent-induced aggregation of the AgNP-NCs was further studied by DLS and TEM (Fig. S5b, S5c, and S5d). The AgNP-NCs in ethanol exhibited obvious aggregations with larger sizes compared with that in water. Based on the AIEE feature, AgNP-NCs can be encapsulated into MOF for having stronger luminescence in water.

AgNP-NCs@ZIF-8 with enhanced luminescence was synthesized and the synthesis conditions was optimized. Fig. S6 presented the effect of dosage of different reactants on PL intensity of AgNP-NCs@ZIF-8, including the molar ratio of 2-MIM to Zn and that of Zn to Ag (concentration of Zn was fixed at 11.5 mM according to previously reported synthesis strategies of ZIF-8 with modification [41]). The molar ratio of 2-MIM to Zn was finally determined to be 3:1 and the molar ratio of Zn to Ag was 17.75:1 according to the maximum photoluminescence intensity of synthesized AgNP-NCs@ZIF-8. The AgNP-NCs@ZIF-8 prepared under optimal synthesis conditions was further characterized in detail. The AgNP-NCs@ZIF-8 exhibited a strong emission peak at 730 nm with a redshift in comparison to that of AgNP-NCs (see Fig. 2a). This redshift was observed at silver nanoclusters/metal-organic shell composites in the previous report [42], which could be caused by the aggregation of AgNP-NCs in MOF. As compared to pure AgNP-NCs, the luminescence intensity of AgNP-NCs@ZIF-8 increased by (66 ± 5) folds (Fig. 2a). To the best of our

knowledge, this luminescence enhancement is the largest among studies on NCs@MOF composites [16-21]. Meanwhile, the intensity of two excitation peaks increased together (Fig. 2a), indicating PEF of AgNP-NCs remained. The obvious luminescence enhancement can be easily observed by naked eyes under 365 nm UV radiation (Fig. 2b). This phenomenon was ascribed to the AIEE of AgNP-NCs caused by spatial confinement of the ZIF-8 shell. The vibrational and rotational non-radiation decays were suppressed by exterior spatially confined scaffold so that more excited electrons decayed with emission. The mechanism was further confirmed by the luminescence lifetimes of AgNP-NCs and AgNP-NCs@ZIF-8. The average lifetime was prolonged from (50.9 ± 1.8) ns to (15.9 ± 0.4) μs after encapsulation by ZIF-8 shell (Fig. 2c, 2d, and Table S1). Such a long photoluminescence lifetime is typically observed in spatially confined metal NCs due to the restricted non-radiation decays [17, 38, 39]. The synergistic effect of PEF and AIEE has been achieved in AgNP-NCs@ZIF-8.

After the AgNP-NCs were encapsulated into the ZIF-8 matrix, the synthesized AgNP-NCs@ZIF-8 exhibited the spherical morphology and aggregated structures compared to pure ZIF-8 (Fig. S7 and 2e). The AgNP-NCs@ZIF-8 composites showed an average diameter of about 40 nm in the TEM image (Fig. 2e). We also obtained the HRTEM image of the AgNP-NCs@ZIF-8 (Fig. 2f). The lattice fringes had a spacing of 0.235 nm, corresponding to the (111) plane of metallic Ag. The spacing of lattice fringes was the same as that of AgNP-NCs (Fig. 2f and S4), further indicating that ZIF-8 encapsulated AgNP-NCs could maintain the structure of AgNP-NCs. CD spectra were also used to characterize the chirality and structure of AgNP-NCs@ZIF-8 (Fig. S8). Compared with ZIF-8, an obvious negative chiral signal appeared at 240 nm in the spectrum of AgNP-NCs@ZIF-8, which proved that chiral AgNP-NCs had successfully embedded in ZIF-8. Due to the combination of AgNP-NCs and Zn^{2+}, the CD signal of AgNP-NCs@ZIF-8 showed a red shift (from 215 nm to 240 nm) compared with that of AgNP-NCs, indicating structural

transformation of AgNP-NCs after encapsulation. Additionally, the FTIR spectra of AgNP-NCs@ZIF-8 and ZIF-8 exhibited high similarity, demonstrating that AgNP-NCs were embedded into ZIF-8 rather than anchored on the surface of ZIF-8 (Fig. S8).

The pH stability of AgNP-NCs@ZIF-8 was also studied in the range of pH 1.8 – 11.5 (Fig. S9a). Photoluminescence intensity of AgNP-NCs@ZIF-8 exhibited a sensitive response to pH, and the maximum intensity was observed at pH 8.5. Thus, the AgNP-NCs@ZIF-8 were used in a weak alkaline environment (pH 8-9.5). TEM images of AgNP-NCs@ZIF-8 at pH 7.5, 8.5, and 11.0 demonstrated the influence of pH on morphology. At pH 8.5, AgNP-NCs@ZIF-8 showed an intact spherical appearance (Fig. S9b). When the solution was adjusted to acidic or neutral, the ZIF-8 shell broke and AgNP-NCs were released, leading to a sharp decline in PL intensity (Fig. S9a and S9c). This hydrolysis phenomenon of ZIF-8 in an acidic environment has been well recognized and applied in drug delivery. [43] While in the alkaline environment, the ZIF-8 shell was reformed into a petal-like structure (Fig. S9d), similar to that previously reported ZIF-8 core-shell composites. [44, 45] This large and thick petal-like shell obstructed luminescence from nanocluster cores, diminishing overall luminescence of the AgNP-NCs@ZIF-8 (Fig. S9a). Due to the luminescence quenching of AgNP-NCs@ZIF-8 in acidic and strongly alkaline environments, pH of the aqueous environment is critical in characterization and application. Thus, pH should be adjusted to a limiting range before testing. And 8.5 was chosen as optimum pH value for further application of AgNP-NCs@ZIF-8.

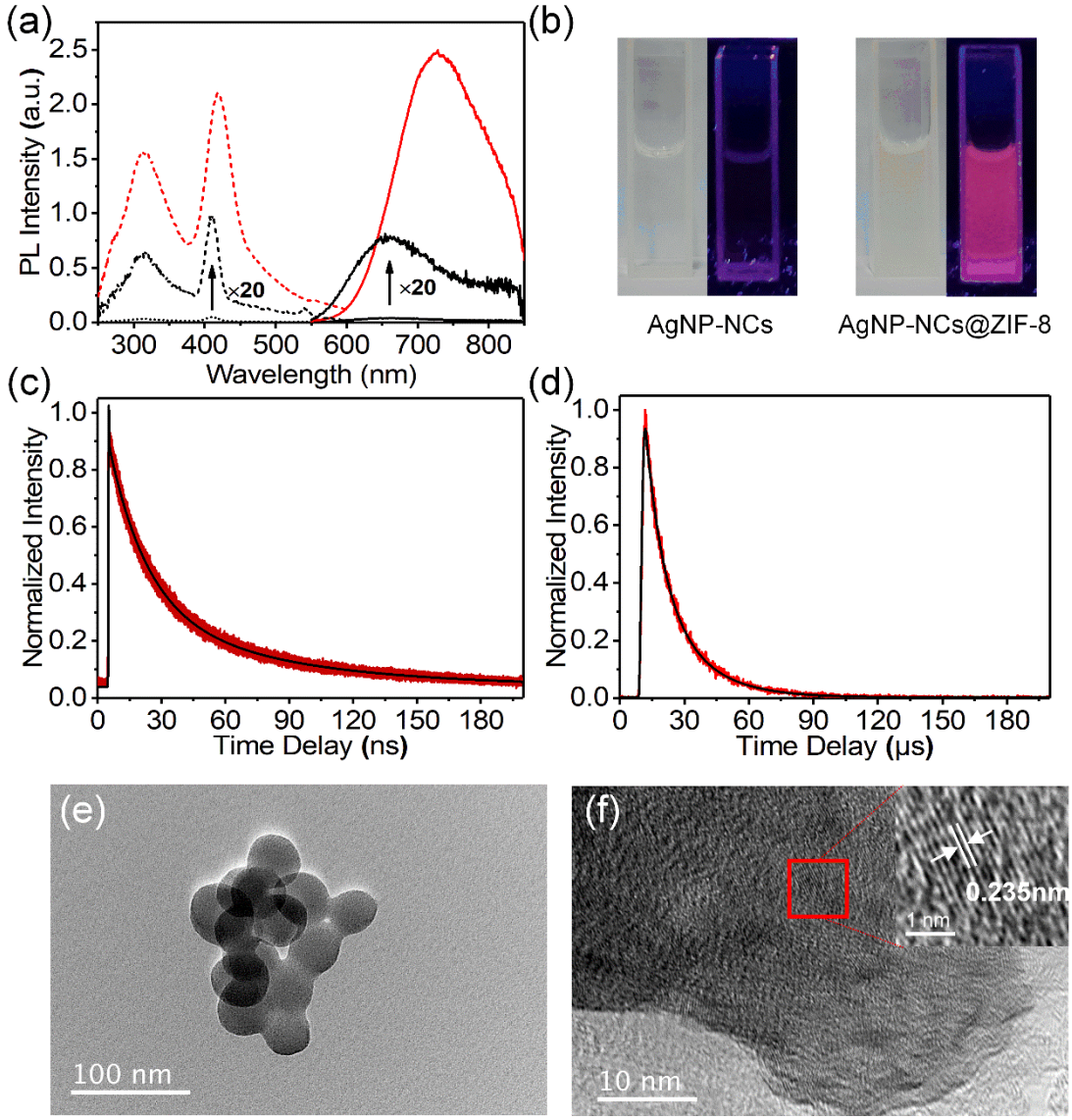

Fig. 2. (a) Excitation (dotted lines) and photoluminescence (PL) spectra (solid lines) of AgNP-NCs (black curves) and AgNP-NCs@ZIF-8 (red curves). Spectra of AgNP-NCs was measured at λ_{ex} = 410 nm, λ_{em} = 665 nm and spectra of AgNP-NCs@ZIF-8 was measured at λ_{ex} = 420 nm, λ_{em} = 730 nm. (b) Photographs of AgNP-NCs and AgNP-NCs@ZIF-8 under visible light and under 365 nm radiation. (c) Normalized PL decays of AgNP-NCs at λ_{ex} = 410 nm, λ_{em} = 665 nm. (d) Normalized PL decays of AgNP-NCs@ZIF-8 at λ_{ex} = 420 nm, λ_{em} = 730 nm. (e) TEM image of AgNP-NCs@ZIF-8. (f) HRTEM image of AgNP-NCs@ZIF-8.

3.3 Detection and removal of chromium(Ⅵ)

The luminescence of AgNP-NCs@ZIF-8 was monitored in the presence of different Cr(Ⅵ) concentrations. The luminescence intensity of the AgNP-NCs@ZIF-8 decreased with increasing Cr(Ⅵ) concentrations ranging from 0 to 2 mM (Fig. 3a). A good linear relationship was observed in the range from 40 μM to 400 μM (Fig. 3b). The linear equation was determined to be $y = 0.00212\ x + 0.14408$, and the correlation coefficient (R^2) was 0.99858. The limit of detection (LOD) was calculated to be (23.5 ± 0.8) μM from $D = 3\sigma/k$ (σ is the standard deviation and k is the slope of calibration line).

To evaluate the Cr(Ⅵ) adsorption performance of the AgNP-NCs@ZIF-8, the typical absorbance of Cr(Ⅵ) was measured at 370 nm to determine the concentration of Cr(Ⅵ) within the adsorption process. The concentration of Cr(Ⅵ) can be determined by the absorbance value because of the good linear relationship between them in a large concentration range (Fig. S10). During the removal process, the absorbance at 370 nm decreased, indicating the successful removal of Cr(Ⅵ) from the water solution (Fig. S11). The plot of adsorption capacity with respect to incubation time was shown in Fig. S12. After 10 h, the adsorption process tended to steady. The adsorption capacity was studied by measuring the absorbance of different Cr(Ⅵ) concentrations before and after incubation with AgNP-NCs@ZIF-8 for 10 h, the AgNP-NCs@ZIF-8 composites were removed by centrifugation before measurements. The adsorption isotherm curve was well fitted by the Langmuir model (R^2=0.96288) (Fig. 3c and S13). The maximum adsorption capacity was calculated to be (7.9 ± 1.3) mg Cr(Ⅵ) per gram of AgNP-NCs@ZIF-8. This capacity was much higher than that of ZIF-8 (0.15 mg/g) [46] and was relatively similar to that of doped ZIF-8 composites, like Co@ZIF-8 (20.7 mg/g) and Ni@ZIF-8 (24.8 mg/g)[45].

Furthermore, we also investigated the selectivity of AgNP-NCs@ZIF-8 for the detection of Cr(Ⅵ) over various interfering metal ions (Na^+, Ca^{2+}, Zn^{2+}, Cr(Ⅲ), Co^{2+},

Cd^{2+}, Ni^{2+}, Pb^{2+}, Cu^{2+}, K^{+}, Mg^{2+}, Mn^{2+}, Fe^{3+}, Ag^{+}, and Hg^{2+}). As shown in Fig. S14, these metal ions had a negligible influence on the luminescence of AgNP-NCs@ZIF-8 except Cu^{2+}, Cr(Ⅲ), and Cr(Ⅵ). Although the luminescence quenching ratio of Cr(Ⅲ) was higher than that of Cr(Ⅵ), AgNP-NCs@ZIF-8 colloidal aqueous solution turned to be clear after the addition of Cr(Ⅲ), indicating that the structure of AgNP-NCs@ZIF-8 was destroyed by Cr(Ⅲ). In addition, Cr(Ⅲ) could be conveniently oxidized to Cr(Ⅵ) for the detection of total chromium, so AgNP-NCs@ZIF-8 was applied for detection and removal of Cr(Ⅵ) rather than Cr(Ⅲ). To shield the interference of Cu^{2+} and oxidize Cr(Ⅲ), the sample solution experienced a pretreatment protocol as mentioned in the experimental section and mixed with AgNP-NCs@ZIF-8 for the selectivity experiment. As shown in Fig. 3d, Cr(Ⅲ) and Cr(Ⅵ) pretreated with H_2O_2 significantly quenched the luminescence of AgNP-NCs@ZIF-8 with a similar quenching ratio, and other competing metal ions still had a negligible influence on the luminescence intensity. Thus, good selectivity toward total chromium was achieved.

The mechanism of the sensitive response of AgNP-NCs@ZIF-8 to Cr(VI) was ascribed to the strong electron transfer, which has been referred in previous reports [47]. The nitrogen atoms on the ligands of the nanoclusters formed hydrogen bonds with the oxygen atoms in Cr(VI). So the electron transfer from Ag nanoclusters as electron donor to Cr(VI), resulting in luminescence quenching.

The interference experiment in the presence of mixed metal ions was carried out, and the results are shown in Fig. S15. The fluorescence intensities of AgNP-NCs@ZIF-8 were not affected by the mixed metal ions, whereas the fluorescence was completely quenched when an equal amount of Cr(Ⅵ) (100 μM) was added into the solutions, further indicating that the interference in Cr(Ⅵ) detection from conventional metal ions could be neglected. The results were also analyzed as shown in Table. S2. The recoveries from 92% to 110% were obtained with relative standard deviations (RSD) less than 4.11%, showing the good

performance of AgNP-NCs@ZIF-8 for Cr(Ⅵ) detection in solutions containing mixed metal ions.

For comparison, the selectivity of pure AgNP-NCs toward Cr(Ⅵ) was also investigated. As shown in Fig. S15, the luminescence of pure AgNP-NCs was quenched by several kinds of metal ions, including Mn^{2+}, Cu^{2+}, Mg^{2+}, Co^{2+}, and Cr(Ⅵ). The sensitivity of pure AgNP-NCs toward Cr(Ⅵ) was much lower than that of AgNP-NCs@ZIF-8. In addition, Mn^{2+}, Mg^{2+}, and Co^{2+} caused an obvious response to the luminescence of AgNP-NCs but exhibited negligible influence to that of AgNP-NCs@ZIF-8. Similarly, the addition of Cr(Ⅲ) led to an obvious quenching of the luminescence of AgNP-NCs@ZIF-8, while no obvious luminescence change of AgNP-NCs was observed. The results indicated that the interaction between Mn^{2+}, Mg^{2+}, Co^{2+}, and AgNP-NCs were blocked after encapsulation, and Cr(Ⅲ) mainly interacted with the MOF shell and therefore had no influence on the luminescence of AgNP-NCs. Compared to pure AgNP-NCs without MOF shells, the luminescence responses of AgNP-NCs@ZIF-8 towards interference metal ions decreased, and the luminescence quenching ratio toward Cr(Ⅵ) increased (Fig. S15 and S17). Therefore, AgNP-NCs@ZIF-8 showed a more sensitive luminescence response and better selectivity toward chromium after encapsulation.

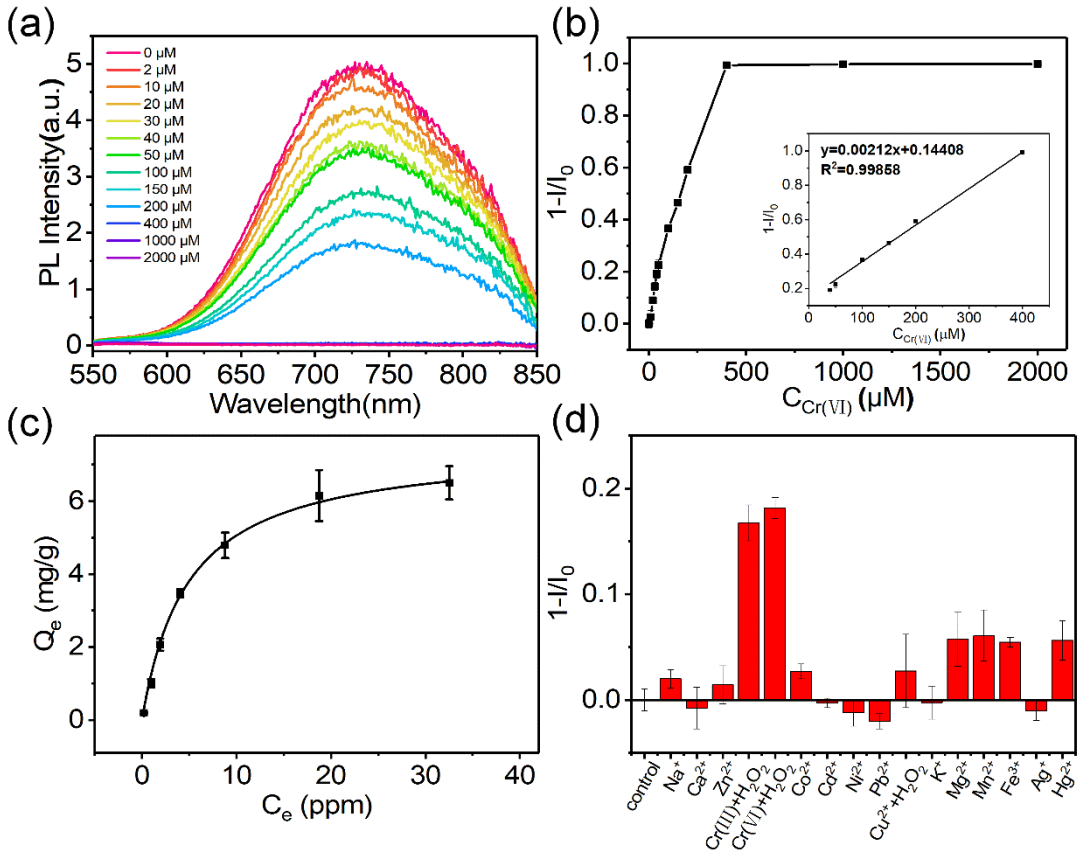

Fig. 3. (a) Photoluminescence spectra of AgNP-NCs@ZIF-8 in the absence and presence of different Cr(Ⅵ) concentrations, λ_{ex} = 420 nm. (b) Plot of luminescence quenching ratio (1 - I/I_0) of AgNP-NCs@ZIF-8 as a function of Cr(Ⅵ) concentration. I_0 and I denote the luminescence intensity of AgNP-NCs@ZIF-8 in the absence and presence of Cr(Ⅵ), respectively. (c) Adsorption isotherm curve for Cr(Ⅵ) adsorption by AgNP-NCs@ZIF-8 at 293 K. Q_e is the adsorption capacity and C_e is the equilibrium concentration. (d) Luminescence quenching ratio of AgNP-NCs@ZIF-8 in the presence of different metal ions, λ_{ex} = 420 nm, λ_{em} = 730 nm. All the metal ions were at 25 μM.

3.4 Application for detection of chromium(Ⅵ) in real samples

To evaluate the practical application of AgNP-NCs@ZIF-8 for the detection of Cr(VI), we performed the experiments in real water samples. Drinking water and tap water were spiked with Cr(VI) solution at known concentrations. As shown in Table S2, the recoveries from 92% to 110% were obtained both in drinking water and tap

water, and the RSDs were less than 13.36%. The result proved minor interference of these samples for the detection of Cr(VI). Therefore, AgNP-NCs@ZIF-8 had good performance in detection of Cr(VI) in real samples.

4 Conclusions

In summary, AgNP-NCs@ZIF-8 composites were prepared and applied for luminescence detection and adsorptive removal of Cr(VI) in water for the first time. Red-emitted DPA-capped AgNP-NCs in the size of ~3 nm were synthesized. The origin of luminescence was ascribed to plasmon-enhanced fluorescence. Then they were encapsulated into a ZIF-8 shell to obtain AgNP-NCs@ZIF-8 composites. AgNP-NCs@ZIF-8 showed an emission peak at 730 nm and excitation peak at 420 nm. The photoluminescence intensity of the AgNP-NCs significantly increased ((66 ± 5) folds) due to the confinement of ZIF-8 via aggregation-induced emission enhancement, and the luminescence lifetime was prolonged from nanoseconds to microseconds (from (50.9 ± 1.8) ns to (15.9 ± 0.4) μs). The AgNP-NCs@ZIF-8 not only allowed for Cr(Ⅵ) detection but also exhibited a good adsorption capacity of Cr(Ⅵ). The luminescence intensity of the AgNP-NCs@ZIF-8 decreased linearly with Cr(Ⅵ) concentrations from 40 to 400 μM, and the LOD was (23.5 ± 0.8) μM. The maximum adsorption capacity calculated by Langmuir model was (7.9 ± 1.3) mg/g. A good selectivity toward total chromium was obtained by sample pretreatments. The recoveries were found to be from 92% to 110% when detecting Cr(Ⅵ) in real water samples. The study opens up a new horizon for NCs@MOF composites in luminescence detection and adsorptive removal of trace contaminants in environmental monitoring and protection.

Declaration of Competing Interest

The authors declare that they have no known competing financial interests or personal relationships that could have appeared to influence the work reported in this paper.

Acknowledgments

This work was supported by the National Natural Science Foundation of China (12174114, 11774096, 21827814, and 21872053), the Research Funds of Happiness Flower ECNU (2021ST2110), and the Fundamental Research Funds for the Central Universities.

Appendix A. Supplementary data

Additional experimental details, including photographs and characterizations of samples (PDF).

References

[1] X. Yuan, Z. Luo, Y. Yu, Q. Yao, J. Xie, Luminescent noble metal nanoclusters as an emerging optical probe for sensor development, Chem. - Asian J. 8 (2013) 858-871.

[2] S. Qian, Z. Wang, Z. Zuo, X. Wang, Q. Wang, X. Yuan, Engineering luminescent metal nanoclusters for sensing applications, Coord. Chem. Rev. 451 (2022) 214268.

[3] X. Kang, M. Zhu, Tailoring the photoluminescence of atomically precise nanoclusters, Chem. Soc. Rev. 48 (2019) 2422-2457.

[4] M.M. Zhang, K. Li, S.Q. Zang, Progress in atomically precise coinage metal clusters with aggregation-induced emission and circularly polarized luminescence, Adv. Opt. Mater. 8 (2020) 1902152.

[5] K. Pyo, V.D. Thanthirige, K. Kwak, P. Pandurangan, G. Ramakrishna, D. Lee, Ultrabright luminescence from gold nanoclusters: rigidifying the Au(I)-thiolate

shell, J. Am. Chem. Soc. 137 (2015) 8244-8250.
[6] N. Kong, H. Yuan, H. Zhou, Y. Zhao, S. Zhang, Colorimetric detection of water content in organic solvents via a smartphone with fluorescent Ag nanoclusters, Anal. Methods 13 (2021) 2722-2727.
[7] S. Basu, H. Fakhouri, C. Moulin, S. Dolai, I. Russier-Antoine, P.-F. Brevet, R. Antoine, A. Paul, Four orders-of-magnitude enhancement in the two-photon excited photoluminescence of homoleptic gold thiolate nanoclusters following zinc ion-induced aggregation, Nanoscale 13 (2021) 4439-4443.
[8] N. Goswami, F. Lin, Y. Liu, D.T. Leong, J. Xie, Highly luminescent thiolated gold nanoclusters impregnated in nanogel, Chem. Mater. 28 (2016) 4009-4016.
[9] M. Li, P. Yuan, Q.-Q. Chen, L.-H. Lin, P.M. Radjenovic, Y.-L. He, J.-Y. Wang, F.-L. Zhang, S.-Y. Luo, N.-F. Zheng, S.-J. Zhang, Z.-Q. Tian, J.-F. Li, Shell-isolated nanoparticle-enhanced luminescence of metallic nanoclusters, Anal. Chem. 92 (2020) 7146-7153.
[10] Y. Zhang, K. Aslan, M.J.R. Previte, C.D. Geddes, Metal-enhanced fluorescence: Surface plasmons can radiate a fluorophore's structured emission, Appl. Phys. Lett. 90 (2007) 053107.
[11] Y. Jiao, Y. Zuo, H. Yang, X. Gao, C. Duan, Photoresponse within dye-incorporated metal-organic architectures, Coord. Chem. Rev. 430 (2021) 213648.
[12] Y. Liu, X. Cao, J. Ge, Antioxidative composites based on multienzyme systems encapsulated in metal-organic frameworks, ACS Appl. Mater. Interfaces 13 (2021) 46431-46439.
[13] Y.X. Li, Y.K. Fu, C. Lai, L. Qin, B.S. Li, S.Y. Liu, H. Yi, F.H. Xu, L. Li, M.M. Zhang, M.Y. Xu, C.Y. Du, W.J. Chen, Porous materials confining noble metals for the catalytic reduction of nitroaromatics: controllable synthesis and enhanced mechanism, Environ. Sci.: Nano 8 (2021) 3067-3097.
[14] Y. Luo, S. Fan, W. Yu, Z. Wu, D.A. Cullen, C. Liang, J. Shi, C. Su, Fabrication of Au25(SG)18 -ZIF-8 nanocomposites: a facile strategy to position Au25(SG)18 nanoclusters inside and outside ZIF-8, Adv. Mater. 30 (2018) 1704576.
[15] L. Luo, R. Jin, Atomically precise metal nanoclusters meet metal-organic frameworks, iScience 24 (2021) 103206.
[16] C. Fan, X. Lv, F. Liu, L. Feng, M. Liu, Y. Cai, H. Liu, J. Wang, Y. Yang, H. Wang, Silver nanoclusters encapsulated into metal–organic frameworks with enhanced fluorescence and specific ion accumulation toward the microdot array-based fluorimetric analysis of copper in blood, ACS Sens. 3 (2018) 441-450.
[17] Q. Gao, S. Xu, C. Guo, Y. Chen, L. Wang, Embedding nanocluster in MOF via crystalline ion-triggered growth strategy for improved emission and selective sensing, ACS Appl. Mater. Interfaces 10 (2018) 16059-16065.
[18] F. Cao, E. Ju, C. Liu, W. Li, Y. Zhang, K. Dong, Z. Liu, J. Ren, X. Qu, Encapsulation of aggregated gold nanoclusters in a metal–organic framework for real-time monitoring of drug release, Nanoscale 9 (2017) 4128-4134.
[19] X. Cao, S. Cheng, Y. You, S. Zhang, Y. Xian, Sensitive monitoring and

bioimaging intracellular highly reactive oxygen species based on gold nanoclusters@nanoscale metal-organic frameworks, Anal. Chim. Acta 1092 (2019) 108-116.

[20] Z. Wang, R. Chen, Y. Xiong, K. Cepe, J. Schneider, R. Zboril, C.-S. Lee, A.L. Rogach, Incorporating copper nanoclusters into metal-organic frameworks: confinement-assisted emission enhancement and application for trinitrotoluene detection, Part. Part. Syst. Charact. 34 (2017) 1700029.

[21] X. Gao, J. Liu, X. Zhuang, C. Tian, F. Luan, H. Liu, Y. Xiong, Incorporating copper nanoclusters into a zeolitic imidazole framework-90 for use as a highly sensitive adenosine triphosphate sensing system to evaluate the freshness of aquatic products, Sens. Actuators, B 308 (2020) 127720.

[22] L. Joseph, B.-M. Jun, M. Jang, C.M. Park, J.C. Munoz-Senmache, A.J. Hernandez-Maldonado, A. Heyden, M. Yu, Y. Yoon, Removal of contaminants of emerging concern by metal-organic framework nanoadsorbents: A review, Chem. Eng. J. 369 (2019) 928-946.

[23] P. Zhuang, P. Zhang, K. Li, B. Kumari, D. Li, X. Mei, Silver nanoclusters encapsulated into metal–organic frameworks for rapid removal of heavy metal ions from water, Molecules 24 (2019) 2442.

[24] L. Zhao, W. Wang, Y. Wang, H. Li, L. Zhao, N. Wang, Y. Wang, X. Wang, Q. Pu, Low-cost devices with fluorescence spots brightness and size dual-mode readout for the rapid detection of Cr(VI) based on smartphones, J. Hazard. Mater. 417 (2021) 125986.

[25] M. Tumolo, V. Ancona, D. De Paola, D. Losacco, C. Campanale, C. Massarelli, V.F. Uricchio, Chromium pollution in european water, sources, health risk, and remediation strategies: an overview, Int. J. Environ. Res. Public Health 17 (2020) 5438.

[26] J. Yoo, U. Ryu, W. Kwon, K.M. Choi, A multi-dye containing MOF for the ratiometric detection and simultaneous removal of $Cr2O7^{2-}$ in the presence of interfering ions, Sens. Actuators, B 283 (2019) 426-433.

[27] A.A. Wani, A.M. Khan, Y.K. Manea, M.A.S. Salem, M. Shahadat, Selective adsorption and ultrafast fluorescent detection of Cr(VI) in wastewater using neodymium doped polyaniline supported layered double hydroxide nanocomposite, J. Hazard. Mater. 416 (2021) 125754-125754.

[28] H.A. Maitlo, K.-H. Kim, V. Kumar, S. Kim, J.-W. Park, Nanomaterials-based treatment options for chromium in aqueous environments, Environ. Int. 130 (2019) 104748.

[29] M. Liu, M. Jia, H. Pan, L. Li, M. Chang, H. Ren, F. Argoul, S. Zhang, J. Xu, Instrument response standard in time-resolved fluorescence spectroscopy at visible wavelength: quenched fluorescein sodium, Appl. Spectrosc. 68 (2014) 577-583.

[30] Y. Chen, T. Yang, H. Pan, Y. Yuan, L. Chen, M. Liu, K. Zhang, S. Zhang, P. Wu, J. Xu, Photoemission mechanism of water-soluble silver nanoclusters: ligand-to-metal-metal charge transfer vs strong coupling between surface plasmon

and emitters, J. Am. Chem. Soc. 136 (2014) 1686-1689.
[31] B.-K.V. Antoine R., Liganded silver and gold quantum clusters: background of their structural, electronic, and optical properties, in: Liganded silver and gold quantum clusters. Towards a new class of nonlinear optical nanomaterials, Springer, Cham, Switzerland, 2018, pp. 5-20.
[32] T. Udayabhaskararao, T. Pradeep, New protocols for the synthesis of stable Ag and Au nanocluster molecules, J. Phys. Chem. Lett. 4 (2013) 1553-1564.
[33] J.F. Li, C.Y. Li, R.F. Aroca, Plasmon-enhanced fluorescence spectroscopy, Chem. Soc. Rev. 46 (2017) 3962-3979.
[34] M. Zhou, C. Zeng, Y. Chen, S. Zhao, M.Y. Sfeir, M. Zhu, R. Jin, Evolution from the plasmon to exciton state in ligand-protected atomically precise gold nanoparticles, Nat. Commun. 7 (2016) 13240.
[35] M. Zhou, R. Jin, Optical properties and excited-state dynamics of atomically precise gold nanoclusters, Annu. Rev. Phys. Chem. 72 (2020) 5.1–5.22.
[36] T. Higaki, M. Zhou, K.J. Lambright, K. Kirschbaum, M.Y. Sfeir, R. Jin, Sharp transition from nonmetallic Au246 to metallic Au279 with nascent surface plasmon resonance, J. Am. Chem. Soc. 140 (2018) 5691-5695.
[37] L. Suber, P. Imperatori, L. Pilloni, D. Caschera, N. Angelini, A. Mezzi, S. Kaciulis, A. Iadecola, B. Joseph, G. Campi, Nanocluster superstructures or nanoparticles? The self-consuming scaffold decides, Nanoscale 10 (2018) 7472-7483.
[38] T. Yang, S. Dai, L. Chen, P. Liu, K. Dong, S. Yang, J. Zhou, Y. Chen, H. Pan, S. Zhang, J. Chen, K. Zhang, P. Wu, J. Xu, Interfacial clustering-triggered fluorescence-phosphorescence dual solvoluminescence of metal nanoclusters, J. Phys. Chem. Lett. 8 (2017) 3980-3985.
[39] N. Goswami, Q. Yao, Z. Luo, J. Li, T. Chen, J. Xie, Luminescent metal nanoclusters with aggregation-induced emission, J. Phys. Chem. Lett. 7 (2016) 962-975.
[40] M. Xia, Y. Sui, Y. Guo, Y. Zhang, Aggregation-induced emission enhancement of gold nanoclusters in metal–organic frameworks for highly sensitive fluorescent detection of bilirubin, Analyst 146 (2021) 904-910.
[41] Y. Pan, Y. Liu, G. Zeng, L. Zhao, Z. Lai, Rapid synthesis of zeolitic imidazolate framework-8 (ZIF-8) nanocrystals in an aqueous system, Chem. Commun. 47 (2011) 2071-2073.
[42] C. Dai, C.X. Yang, X.P. Yan, Ratiometric fluorescent detection of phosphate in aqueous solution based on near infrared fluorescent silver nanoclusters/metal-organic shell composite, Anal. Chem. 87 (2015) 11455-11459.
[43] A. Maleki, M.-A. Shahbazi, V. Alinezhad, H.A. Santos, The progress and prospect of zeolitic imidazolate frameworks in cancer therapy, antibacterial activity, and biomineralization, Adv. Healthcare Mater. 9 (2020) 2000248.
[44] J. Cui, Y. Feng, T. Lin, Z. Tan, C. Zhong, S. Jia, Mesoporous metal–organic framework with well-defined cruciate flower-like morphology for enzyme immobilization, ACS Appl. Mater. Interfaces 9 (2017) 10587-10594.

[45] B. Shen, B. Wang, L. Zhu, L. Jiang, Properties of cobalt- and nickel-doped ZIF-8 framework materials and their application in heavy-metal removal from wastewater, nanomaterials 10 (2020) 1636.

[46] M. Niknam Shahrak, M. Ghahramaninezhad, M. Eydifarash, Zeolitic imidazolate framework-8 for efficient adsorption and removal of Cr(VI) ions from aqueous solution, Environ. Sci. Pollut. Res. 24 (2017) 9624-9634.

[47] J.R. Zhang, A.L. Zeng, H.Q. Luo, N.B. Li, Fluorescent silver nanoclusters for ultrasensitive determination of chromium(VI) in aqueous solution, J. Hazard. Mater. 304 (2016) 66-72.